

PAHs in circumstellar disks around Herbig Ae/Be stars[★]

E. Habart¹, A. Natta¹, and E. Krügel²

¹ Osservatorio Astrofisico di Arcetri, INAF, Largo E. Fermi 5, 50125 Firenze, Italy

² Max-Planck Institute für Radioastronomie, Auf dem Hügel 69, Bonn, Germany

Received 19 December 2003 / Accepted 17 June 2004

Abstract. We investigate the presence and properties of PAHs on the surface of circumstellar disks around Herbig Ae/Be stars by comparing the predictions of disk models with observations. We present results of a radiation transfer code for disks heated by the central star, in hydrostatic equilibrium in the vertical direction (flared disks). The dust is a mixture of large grains in thermal equilibrium, transiently heated small grains and PAHs. Special attention is given to the influence of the stellar, disk and PAH properties on the strength of the PAH emission lines and their spatial distribution. The models predict an infrared SED showing PAH features at 3.3, 6.2, 7.7, and 11.3 μm clearly visible above the continuum, and with some of them very strong. The PAH emission, spatially extended, comes mostly from the outer disk region ($R \sim 100$ AU) while the continuum emission at similar wavelengths, mostly due to warm large grains, is confined to the innermost disk regions ($R \sim \text{few AU}$). We compare the model results to infrared observations from ISO and ground-based telescopes of some thirty Herbig Ae/Be stars. Most of the observed PAH features in objects with spectral type later than B9 are well described by our disk models and we discuss in some detail the PAH characteristics one can derive from the existing data. Objects with strong radiation field (generally earlier than about B9) have the 3.3 μm feature (often the only one observed) much weaker than predicted, and we discuss possible explanations (dissipation of the disk, photoevaporation or modification of the PAH properties).

Key words. stars: circumstellar matter – stars: pre-main sequence – ISM: dust, extinction – radiative transfer – infrared: ISM – ISM: lines and bands

1. Introduction

Features of PAHs (Polycyclic Aromatic Hydrocarbons) are detected in a number of pre-main-sequence stars of intermediate mass with circumstellar disks, with characteristics that differ from those in the interstellar medium (see, e.g., Van Kerckhoven et al. 2002). An origin of these features in the disk surface layers, which are directly exposed to the ultraviolet (UV) stellar radiation, has been suggested by various authors (see, e.g., Meeus et al. 2001). Recently, PAH emission has been resolved spatially in HD 100546, HD 97048 (van Boekel et al. 2004) and WL 16 (Moore et al. 1998; Ressler & Barsony 2003), and shown to have the size typical of circumstellar disk emission.

The presence of PAHs on disk surfaces is interesting for a number of reasons. First of all, as we will see in the following, PAHs are good tracers of the presence of very small particles mixed with the gas at large altitudes above the disk midplane, both near the star and in the very outer disk. Their emission can tell us if and where very small particles survive settling and coagulation processes that cause the majority of the original grain population to grow to very large sizes in the same objects (see, e.g., Natta & Testi 2003). A second point of interest is that the absence or presence of PAHs will have a significant impact on

the physical properties of the gas and on the structure of the disk itself, since in photo-dissociation regions we believe that they contribute a large fraction of the gas heating (via the photoelectric effect, see, e.g., Weingartner & Draine 2001; Habart et al. 2001) and could dominate the H_2 formation on dust surfaces (Habart et al. 2004).

The presence and properties of PAHs in circumstellar disks can be tested by comparing the observations with the predictions of disk models, which have been shown to reproduce well the global spectral energy distribution (SED) of the same stars (Dullemond et al. 2001; Dominik et al. 2003). We are interested in particular to check if the disk models can account for the observed intensity of the various features and their spatial distribution, when known. To the best of our knowledge, there are no such models available for disks around pre-main-sequence stars. These disks are optically thick to the stellar radiation and thus require a proper treatment of the radiation transfer. Recent models of the SED of HD 141569A (a young B9.5 star with a complex debris disk) by Li & Lunine (2003), which include PAHs, assume an optically thin disk, as appropriate for that particular object.

The paper is organized as follows. Section 2 provides a summary of the available observations of PAHs in intermediate-mass stars. The disk models and the radiation transfer scheme we use are described in Sects. 3.1 and 3.2. The dust on the disk surface is a mixture of large grains, which

[★] Appendix is only available in electronic form at <http://www.edpsciences.org>

Table 1. Parameters of Herbig Ae/Be candidates. Evidence for a flared disk and disk outer radius from spectral energy distribution modeling and millimeter interferometry observations. Presence of AIBs and silicate bands. Crystalline signatures.

Object	d [pc]	Sp. type	T_{eff} [K]	L_{\star} L_{\odot}	χ^a	Flared disk	R_{disk}^b [AU]	AIBs	Sil.	Cryst.	Ref.
AB Aur	144	B9/A0Ve	9750	47	10^5	√	140	√	√	–	(1)
HD 100 546	103	B9Ve	11 000	36	10^5	√	300(150 ^{b1})	√	√	√	(1)
HD 142 527	200	F7IIIe	6250	31	4×10^3	√		√	√	√ ^c	(1)
HD 179218	240	B9e	10 000	80	2×10^5	√	(<600 ^{b2})	√	√	√ ^c	(1)
HD 100453	114	A9Ve	7500	9	5×10^3	√		√	–	–	(1)
HD 135344	84	F4Ve	6750	3	6×10^2	√		?	–	–	(1)
HD 139614	157	A7Ve	8000	12	10^4	√		–	–	–	(1)
HD 169142	145	A5Ve	10 500	32	10^5	√	220	√	–	–	(1)
HD 104237	116	A4Ve	10 500	40	10^5	No		–	√	?	(1)
HD 142666	116	A8Ve	8500	11	10^4	No		√	√	√ ^c	(1)
HD 144432	200	A9Ve	8000	32	3×10^4	No		–	√	?	(1)
HD 150193	150	A1Ve	10 000	40	10^5	No		–	√	√	(1)
HD 163296	122	A3Ve	10 500	30	10^5	No	360	–	√	√	(1)
HD 97048	180	B9-A0	10 000	31	10^5		(300 ^{b1} –900 ^{b2})	√	–	–	(2)
Elias I	150	A0-A6	8000	21	2×10^4		70 (<200 ^{b3})	√	√	? ^d	(2)
Lk H α 25	800	A0	9800	9	2×10^4		(<1200)	√	–	–	(3)
HK Ori	460	A5	8300	12	10^4		(70)	√	–	–	(3)
HD 245185	400	A2	9100	17	3×10^4		(110)	√	–	–	(3)
Lk H α 198	600	A5	8300	6	6×10^3		(900)	–	√	–	(3)
BD+61°154	650	B8	11 200	330	10^6		(900)	–	–	–	(3)
T Ori	460	B9	10 700	83	3×10^5		(88)	–	–	–	(3)
V380 Ori	460	B9	10 700	85	3×10^5		(150)	–	√	–	(3)
HD 250550	700	B7	12 300	240	10^6		(410)	–	–	–	(3)
Lk H α 208	1000	B7	12 300	210	10^6		(1600)	–	–	–	(3)
VV Ser	440	B9	10 700	100	4×10^5		(410)	–	–	–	(3)
WW Vul	700	A3	8700	20	3×10^4		(88)	–	–	–	(3)
BD+46°3471	1000	A0	9800	508	10^6		(190)	–	–	–	(3)
Lk H α 233	880	A5	8300	30	3×10^4		(320)	–	√	–	(3)
WL 16	125	B8-A7	9000	240	4×10^5		(450)	√	–	–	(4)

√ : detection, ? : possible detection, – : no detection.

^a Far-ultraviolet (FUV, $6 < h\nu < 13.6$ eV) flux at 150 AU from the star expressed in units of the average interstellar radiation field, 1.6×10^{-6} W m⁻² (Habing 1968).

^b In parentheses we give estimate of the PAH emission extension. References: (b1) van Boekel et al. (2004); (b2) Siebenmorgen et al. (2000); (b3) Brooke et al. (1993).

^c Possible blend with the PAH 11.2(3) μ m band.

^d Hanner et al. (1994).

References: (1) Meeus et al. (2001) and references therein; (2) Van Kerckhoven et al. (2002) and references therein; (3) for astrophysical parameters Hillenbrand et al. (1992) (except for BD+46°3471 see Berrilli et al. (1992) and for VV Ser see Testi et al. (1998)); for PAH emission extension and AIBs detection Brooke et al. (1993); for silicate emission features detection Berrilli et al. (1992); (4) Ressler & Barsony (2003) and references therein.

reach equilibrium with the stellar radiation field, very small grains, and PAHs, which are transiently heated by the UV stellar radiation. The details of the adopted dust model are given in Sect. 3.3. The results of the calculations are described in Sect. 4, which also explores the effect of varying the stellar, disk and PAHs properties. In Sect. 5 we compare the model results to the observations. Sect. 6 summarizes our main results.

2. Summary of the observations

From ground-based and airborne observations (Brooke et al. 1993; Schutte et al. 1990), it is known that aromatic infrared

emission bands (AIBs in the following) attributed to PAHs exist in the spectra of some Herbig Ae/Be stars (hereafter HAeBe). About 20% of the HAeBe stars surveyed to date have a firmly detected 3.3 μ m feature (Brooke et al. 1993).

In Table 1, we report for an ISO sample of HAeBe stars with circumstellar disks (i) the astrophysical parameters of each star (distance, spectral type, effective temperature, luminosity, and χ , i.e., FUV flux at 150 AU from the star), (ii) the observational characteristics of the disk (evidence for a flared disk and disk outer radius) and (iii) the dust spectral characteristics (presence of AIBs, silicate bands and crystalline signatures). We also give, when available, estimates of the extension

Table 2. Integrated strength of the PAH emission features.

Object	3.3 [μm]	6.2 [μm]	“7.7” [μm]	8.6 [μm]	11.2(3) [μm]	12.7 [μm]	16.4 [μm]	Ref.
AB Aur	<1 ^a	4.4(0.3)	4.2(0.6)	2(0.2)	2(0.6)	–	–	(1)
HD 100546	2.5(0.5)	14.3(0.4)	19.2(0.8)	4.6(0.5)	– ^b	–	–	(1)
HD 142527	1(0.6)	<1.5	–	–	<0.5	–	–	(1)
HD 179218	1.7(0.2)	8.1(0.4)	14.4(0.6)	1.6(0.4)	–	–	–	(1)
HD 100453	1.3(0.2)	2.6(0.5)	–	–	1.2(0.3)	–	–	(1)
HD 135344	<0.5	<1.5	?	–	<1	–	–	(2)
HD 139614	<0.5	<1.5	–	–	<0.5	–	–	(2)
HD 169142	1(0.2)	2.8(0.3)	–	–	2.3(0.5)	–	–	(1)
HD 104237	<0.5	<1.5	–	–	–	–	–	(2)
HD 142666	0.3(0.2)	2.6(0.3)	–	–	–	–	–	(1)
HD 144432	<0.5	<1.5	–	–	–	–	–	(2)
HD 150193	< 0.08 ^a	<1.5	–	–	–	–	–	(2)
HD 163296	<0.2 ^a	<1.5	–	–	–	–	–	(2)
HD 97048	1.3(0.3)	6.9(0.8)	11.8(1.3)	2.4(0.6)	3.4(0.4)	1(0.2)	–	(2)
Elias 1	0.5 ^c (0.1)	6.1(0.6)	9.4(0.1)	2.3(0.1)	– ^d	–	–	(2)
Lk H α 25	0.076(0.006)							(3)
HK Ori	0.087(0.045)							(3)
HD 245185	0.035(0.018)							(3)
Lk H α 198	<0.15							(3)
BD+61°154	<0.09							(3)
T Ori	<0.15							(3)
V380 Ori	<0.1							(3)
HD 250550	<0.12							(3)
Lk H α 208	<0.03							(3)
VV Ser	<0.05							(3)
WW Vul	<0.09							(3)
BD+46°3471	<0.1							(3)
Lk H α 233	<0.04							(3)
WL 16	0.17(0.03)				5(0.4)			(4)

Integrated fluxes (after continuum subtraction) and uncertainty (in between brackets) are in units of 10^{-14} W/m². For non-detections, we give for the 3.3, 6.2 and 11.3 μm feature 5σ limits estimated from the spectrum of Meeus et al. (2001) and assuming constant feature widths taken from Li & Draine (2001a). We have not included the 11.2(3) μm band for the sources with strong silicate emission.

^a From Brooke et al. (1993).

^b In the spectrum of HD 100546 a 11.2(3) μm PAH feature is present but may be blended with the crystalline olivine band at 11.3 μm (Malfait et al. 1998).

^c Measured in ground-based spectrum (Geballe 1997).

^d Hanner et al. (1994) report the presence of an 11.2 μm feature in their UKIRT spectrum. They attribute this feature to the presence of crystalline silicate but it could also be a PAH band.

References: (1) Van Kerckhoven et al. (2002); (2) Meeus et al. (2001); (3) Brooke et al. (1993); (4) From the spectrum of Tokunaga et al. (1991) and Hanner et al. (1992) for the 3.3 and 11.3 μm feature, respectively.

of the PAH emission. The strengths of the PAH emission features at 3.3, 6.2, 7.7, 8.6, 11.2(3), 12.7 and 16.4 μm (where most commonly observed PAH features occur) are given in Table 2. Most of these sources are *isolated* HAeBe stars, with the exception of two objects, HD 97048 and Elias 1, which are still embedded in a reflection nebula. These sources are intermediate between embedded and isolated HAeBe stars. In Tables 1 and 2 we also report the characteristics of the HAeBe stars observed at 3 μm by Brooke et al. (1993) and of the young stellar object WL 16 embedded in the ρ Ophiuchi cloud core (for a recent paper see Ressler & Barsony 2003).

In the ISO sample of isolated HAeBe stars we can distinguish three different groups (Meeus et al. 2001): the first (group Ia) is made of stars with evidence of a flared disk and

strong or moderately aromatic and silicate bands (with or without crystalline signatures); the second (group Ib) is also characterised by flared disks and the presence of AIBs, but the silicate bands are absent; finally, in the third group (group II) there is no evidence of a flared disk, there are weak or no AIBs, but the silicate emission features are strong (with various amounts of crystalline silicates). The presence of AIBs is not correlated with any of the stellar parameters. There is, on the other hand, an indication that PAH features are strong when disks are flared, since they are present in group I objects (both Ia and Ib) and only (and rather weakly) in one source of group II. This suggests that PAH emission originates in the outer regions of flared disks, where dust intercepts a large fraction of the UV emission coming from the star.

That in isolated HAeBe stars PAHs must be closely related to the star-disk system is supported by the observations of HD 100546 and HD 179128 (both group Ia) showing that the PAH emission occurs within ~ 150 AU (Grady et al. 2001; van Boekel et al. 2004) and ~ 600 AU (Siebenmorgen et al. 2000) from the star, respectively. Moreover, van Boekel et al. (2004) find that HD 104237 (group II) is unresolved in their $10 \mu\text{m}$ spectroscopic observations using TIMMI2 at the ESO 3.6-m telescope with a spatial resolution of $\sim 0.9''$. This is consistent with the idea that group II sources do not possess a flared outer disk. As far as we know, no spatial information on the PAH emission is available for the other isolated HAeBe stars but their isolated nature suggests that also in these objects the PAH emission comes from the immediate circumstellar environment. On the other hand, for the two intermediate sources, HD 97048 and Elias 1, the PAH emission probably originates in a significant part from the illuminated reflection nebula. HD 97048 observations show that the PAH emission extends up to ~ 1000 AU (Siebenmorgen et al. 2000). However, recent high spatial resolution observations show that most of the emission of the 8.6 , 11.3 and $12.7 \mu\text{m}$ features comes in fact from a region of 200 – 300 AU, likely a disk (van Boekel et al. 2004). Additional evidence of the PAH emission disk origin in HAeBe stars comes from recent (sub)arcsec-resolution mid-IR images of WL 16 by Moore et al. (1998); Ressler & Barsony (2003), showing that the PAH emission has a size of ~ 450 AU. Finally, note that for the HAeBe stars observed from the ground at $3 \mu\text{m}$, Brooke et al. (1993) find that the aromatic features tend to be confined to ~ 1000 AU.

It is also interesting that in HD 97048 and WL 16 the $10 \mu\text{m}$ continuum emission is spatially extended on scales comparable to those of the PAH emission (van Boekel et al. 2004; Moore et al. 1998; Ressler & Barsony 2003). Together with the absence of the spectral signature of silicate grains in both these sources (see references in Table 1), this indicates that very small carbonaceous grains are responsible for the continuum emission. Quite differently, the continuum emission in HD 100546 arises from a much smaller (< 30 AU) region than the PAH emission (van Boekel et al. 2004). In this object, where silicate bands are present, the continuum may be dominated by warm large silicates grains confined to the innermost regions of the disk.

Evidence of a disk origin of the PAH emission in HAeBe stars comes also from the extensive study of the ISO spectra of a sample of embedded young stellar objects, isolated HAeBe stars, evolved stars, reflection nebulae and HII regions, which reveals the presence of variations in the profiles and peak positions of the main bands from source to source (Hony et al. 2001; Van Kerckhoven et al. 2002; Peeters et al. 2002). The largest variation is seen in the 6 – $9 \mu\text{m}$ region with systematic differences between sources that have recently synthesized their PAHs in their ejecta and sources that are illuminating general interstellar medium materials (Peeters et al. 2002). The combined effect of PAH family and anharmonicity (dependence of the peak position on the temperature of the emitters) could be at the origin of these variations. The 6.2 and $7.7 \mu\text{m}$ features in isolated HAeBe stars which resemble those in evolved stars are very different from those in sources with

ISM material. Moreover, large variations are observed in the ratio of the band strengths in the 10 – $15 \mu\text{m}$ region, especially in the $11.2/12.7 \mu\text{m}$ ratio (Hony et al. 2001). Together with the good correlation found between the 11.2 and $3.3 \mu\text{m}$ band and between the 12.7 and $6.2 \mu\text{m}$ band, Hony et al. (2001) suggest that the spectra of HII regions where the 11.2 and $12.7 \mu\text{m}$ are typically equally strong are due to small or irregular (and preferentially ionized) PAHs. On the other hand, the spectra of evolved stars with a small $12.7/11.2 \mu\text{m}$ ratio may arise from large (~ 100 – 150 C-atom) compact (and preferentially neutral) PAHs. The $12.7 \mu\text{m}$ band cannot be seen in the low resolution spectra of isolated HAeBe stars and the $12.7/11.2 \mu\text{m}$ ratio is not known. But recent ground-based observations (see reference in Van Kerckhoven et al. 2002) confirm that, if present, the $12.7 \mu\text{m}$ band must be very weak compared to the $11.2 \mu\text{m}$ band. This indicates that the PAHs are larger and less ionized in isolated HAeBe sources.

In summary, there are indications that PAHs in HAeBe stars are somewhat different from those in the ISM, and more similar to PAHs in evolved stars. However, it is difficult to fully characterize the PAH properties in HAeBe stars from what is known at present, and in the following we will start our analysis from the assumption that PAHs in the ISM represent a good first approximation to the properties of PAHs in disks as well. We will then discuss possible differences, and come back to this point in our conclusions.

3. Models

In this section, we describe the disk models and the radiation transfer used and give the details of the adopted dust model.

3.1. Disk models

We consider disks heated by irradiation from the central star, in hydrostatic equilibrium in the vertical direction, with gas and dust well mixed (flared disks). We compute the disk structure using an improved version of the Chiang & Goldreich (1997) two-layer models, described in Dullemond et al. (2001). For a given star, the disk structure (i.e., pressure scale height H_p and flaring angle α) is completely defined once the inner and outer radii (R_{in} and R_{d}), the surface density distribution $\Sigma = \Sigma_0(R/R_0)^{-p}$ with R_0 a fiducial radius, and the dust model are specified.

In these models, the stellar flux impinging with flaring angle α upon the disk is absorbed in the upper layers of the disk, which will reradiate half of the flux away from the disk and half down into its deeper layers. Here, we compute the structure of the disk self-consistently using an iterative scheme that gives the flaring angle α and the midplane temperature at each radius. The radiation transfer is solved in an effective, simplified way, which, however, gives a disk structure very similar to that obtained with a full, much more time consuming radiation transfer treatment (Dullemond & Natta 2003).

The models are appropriate for disks that are optically thick to the stellar radiation. This is generally the case for disks around pre-main-sequence stars, up to very large radii (e.g., 5000 AU for a disk mass $M_{\text{d}} \sim 0.2 M_{\odot}$, $p = 1$).

3.2. Radiative transfer

In spite of the success of the two-layer codes in predicting the disk structure and the overall SED, they tend to overestimate the disk emission in the near-infrared (Dullemond & Natta 2003). We have therefore decided to implement a full 1D radiation transfer scheme to compute more accurately the emission in the wavelength range where the PAH features occur. In practice, we first compute the disk structure using our two-layer code, with the adopted dust model (which includes transiently heated species), then, the disk structure fixed, we compute the emerging spectrum using the radiation transfer code. This procedure is not fully self-consistent, but we have checked that it does not introduce any significant inaccuracy in our results.

Dust scattering is incorporated. Scattering of stellar light may be relevant because it can lead to a substantial reduction of the flux available for heating the disk and because it allows stellar photons, after one scattering event, to penetrate much deeper into the disk than one would expect given the smallness of the flaring angle α .

To calculate the emission of transiently heated small grains and of PAHs, we compute the temperature distribution functions dP/dT as in Siebenmorgen et al. (1992) following the method outlined by Guhathakurta & Draine (1989).

To determine the emission from the disk, we divide it into rings of radius r and small radial width Δr . At the center, at $r = 0$, sits the star with parameters M_\star , L_\star , R_\star and T_{eff} . For each ring we compute, as described in the appendix, the radiative transfer perpendicular to the disk, in the z -direction, and then add up the contributions from all rings.

3.3. Dust model and PAH properties

The properties of dust in circumstellar disks differ significantly from those in the ISM (see Sect. 2), and from star to star. It is difficult to build a general, realistic dust model. However, this is not the purpose of this study, where we only want to test the hypothesis that the observed PAH features have their origin in the surface layers of circumstellar disks. Therefore, we will start with a dust model that includes large grains (i.e., grains large enough to be in thermal equilibrium with the local radiation field) with properties that roughly account for the observed SEDs (including the silicate emission at $10\ \mu\text{m}$) of most pre-main-sequence stars. To these, we will add very small particles and PAHs, with abundances and properties typical of the ISM, which we will then vary.

a) Large grains. The large or big grains (BGs in the following) consist of graphite and silicates with optical constants from Draine (1985). These grains have an MRN size distribution ($n(a) \propto a^{-3.5}$) between a minimum and a maximum radius $a_l = 0.01\ \mu\text{m}$ and $a_u = 0.74\ \mu\text{m}$ for silicates and $a_l = 0.01\ \mu\text{m}$ and $a_u = 0.36\ \mu\text{m}$ for graphite. We assume that all silicon and about 2/3 of the cosmic carbon¹ ($[C/H]_{\text{BGs}} = 1.5 \times 10^{-4}$) are

in these grains. This prescription gives a good fit to the mid-IR SED (which originates from the disk surface) of many H Ae stars (Natta et al. 2001); we have found in our modeling that the details are not very important for the purpose of this paper.

b) Very small grains. To the BGs population of grains, we add a tail of very small graphite particles (VSGs in the following) with the same size distribution $n(a) \propto a^{-3.5}$ between $a_l = 10\ \text{\AA}$ to $a_u = 100\ \text{\AA}$. Optical constants are from Draine (1985). The fraction of carbon in VSGs is 15% of that in BGs ($[C/H]_{\text{VSGs}} = 0.22 \times 10^{-4}$). VSGs and BGs graphite grains probably form a continuous population. The division between BGs and VSGs is maintained mainly for computational purposes. Note that there is no evidence in the ISM of very small silicates (Li & Draine 2001b).

c) PAHs. Finally, we include in our dust model a population of PAHs. In the ISM, PAHs are made up of a few tens up to a few hundreds of carbon atoms; for reasons of simplicity, we start our models with one PAH size, $N_C = 100$. The hydrogen to carbon ratio is $H/C = f_H \times (6/N_C)^{0.5}$ (case of compact symmetric PAHs, see Omont 1986) with f_H the hydrogenation fraction of the molecule. We start our models assuming essentially fully hydrogenated PAHs, i.e. $f_H = 1$. The carbon locked up in PAHs has an abundance of $[C/H]_{\text{PAH}} \approx 5 \times 10^{-5}$ inferred from the $12\ \mu\text{m}$ emission per hydrogen atom in typical Galactic cirrus (Boulanger & Perault 1988) and photo-dissociation regions (Habart et al. 2001) and from comparison between observations of dust galactic emission and extinction with detailed model calculations (Désert et al. 1990; Dwek et al. 1997; Li & Draine 2001a). We take the absorption cross section as defined by Li & Draine (2001a) based both on laboratory data and astrophysical spectra. They consider the bands at 3.3, 8.6, 11.3, 11.9 and $12.7\ \mu\text{m}$ from vibrational modes of the aromatic C-H bond; the strong bands at 6.2 and $7.7\ \mu\text{m}$ due to vibrations of the aromatic C-C bonds; and a few weak features probably caused by C-C bending modes at 16.4, 18.3, 21.2 and $23.1\ \mu\text{m}$. The band profiles have a Drude shape; the integrated cross sections band profiles, positions and widths of the lines are found in their Table 1². The cross section in the visible UV is determined from the laboratory absorption spectrum of small species with a cut-off in the visible to near-IR whose wavelength increases with N_C , as defined by Désert et al. (1990).

With respect to the charge, we start assuming that PAHs are mostly neutral. Ideally, one can calculate the steady state charge distribution of PAHs from the balance between electron capture rates and the photoelectron emission rates plus the ion capture rates (see, e.g., Weingartner & Draine 2001). Since little is known regarding the electron density n_e and its distribution in the surface layers of disks, precise determination of the PAH charge distribution in disks is not possible. Instead, we can estimate the ratio between the photoionisation rate of

² To fit the observed IR spectrum of the diffuse ISM, Li & Draine (2001a) include enhancement factors $E_{6.2}$, $E_{7.7}$ and $E_{8.6}$ in the integrated cross sections for the 6.2, 7.7 and $8.6\ \mu\text{m}$ bands. For the template model, we adopt $E_{6.2}$, $E_{7.7}$, $E_{8.6}$ equal to 1, which recover typical laboratory values, but we will also consider the model with $E_{6.2}$, $E_{7.7}$, $E_{8.6} > 1$ (see Sect. 4.2.5).

¹ Snow & Witt (1995) discussed the carbon abundance in stars newly formed from the ISM and conclude that the carbon abundance in the local ISM is $(2.24 \pm 0.5) \times 10^{-4}$.

the grain to the electron-grain recombination rate, γ , which can be approximated by $\gamma_0 \times f(N_C) N_C^{2/3} \times \chi T_{\text{gas}}^{1/2}/n_e$ with $f(N_C)$ a function giving the dependence of the photo-electron ejection probability with the size (see Bakes & Tielens 1994). For a disk heated by a typical H Ae star, we have $\chi \sim 10^5$ and $n_H \sim 10^7 \text{ cm}^{-3}$ on the surface disk layer at 150 AU from the star (see next section). Thus, assuming $n_e/n_H \sim 1.5 \times 10^{-4}$ (as in typical photo-dissociation regions of the ISM) and $T_{\text{gas}} \sim 100 \text{ K}$, we find $\chi T_{\text{gas}}^{1/2}/n_e \sim 500$ and for a PAH with $N_C \sim 100$ we estimate³ that γ is less than 1. This implies that PAHs must be neutral or negatively charged in the outer disk regions. In the inner disk region and for stars with higher χ , however, γ becomes higher and PAHs will be in part positively charged. To keep the model simple, we neglect that we probably have a mixture of neutral and charged PAHs in disks and we assume that PAHs are neutral. The effect of charge is briefly discussed in Sect. 4.2.1.

Upon absorption of an energetic photon, small PAHs, with an insufficient number of internal vibrational modes in which to distribute this photon energy, may dissociate. In a strong FUV radiation field ($\chi > 10^2$), destruction occurs during multiphoton events where PAHs absorb an energy of more than 21 eV in a time shorter than the cooling time (Guhathakurta & Draine 1989; Siebenmorgen 1993). Recently, Li & Lunine (2003) estimated the photodestruction rate for the HD 141569A disk and suggest that PAHs with $N_C \leq 40\text{--}50$ will be photolytically unstable in the inner $R < 100 \text{ AU}$ region around the star (where $\chi > 10^5$) during the life time of the disk. For a PAH with $N_C \sim 40\text{--}50$, the maximum temperature reached just after the deposit of an energy of 21 eV is about 2000 K (see, e.g., Omont 1986). In our model, we assume that PAHs are destroyed when the probability that they are at a temperature $T \geq T_{\text{evap}}$ exceeds a critical value p_{evap} , i.e., when $\int_{T_{\text{evap}}}^{\infty} P(T)dT \geq p_{\text{evap}}$. This procedure is numerically simple and can probably correctly evaluate evaporation. However, we do not derive p_{evap} from thermodynamical considerations. We used $T_{\text{evap}} = 2000 \text{ K}$ and $p_{\text{evap}} = 10^{-8}$ and checked that for this choice, in the case of small PAHs, the results are similar to the assumption that the grains are photo-destructed if they absorb an energy of more than 21 eV in a time interval shorter than the cooling time.

In summary, we adopt a dust model with BGs, VSGs and PAHs. The silicate abundance in dust is $[\text{Si}/\text{H}] = 3 \times 10^{-5}$, and the total carbon abundance in dust is $[\text{C}/\text{H}] = 2.22 \times 10^{-4}$. Of this, 23% is in PAHs, 10% in VSGs and 67% in large grains. Figure 1 shows the adopted absorption coefficient for the various species. For a radiation field that has a blackbody distribution at $T = 10^4 \text{ K}$, BGs will absorb 50% of the radiation, VSG 11% and PAHs 39%, respectively. The properties of BGs are somewhat different from those of grains in the ISM, and have been chosen to approximately fit the properties of dust on disk surfaces. VSGs and PAHs have properties derived from the ISM. In the following, however, we will explore the effects on the predicted spectra of some of our assumptions for the PAHs properties. Note, however, that we will not try to reproduce the peculiarities of the features observed in some isolated

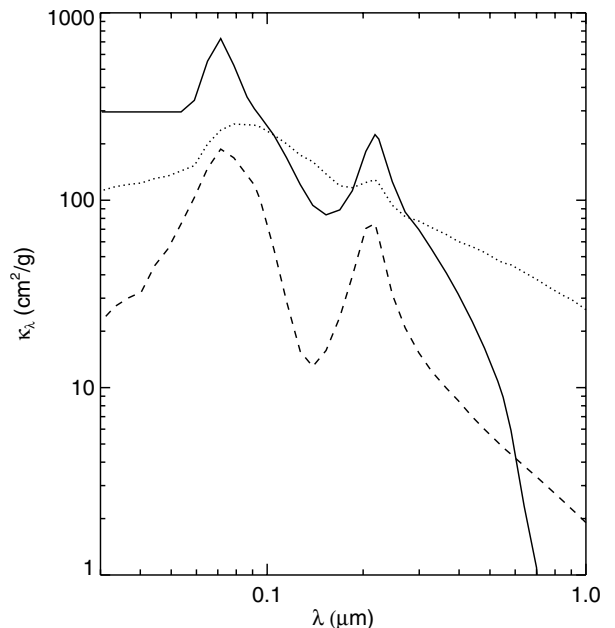


Fig. 1. Absorption coefficient (in cm^2 per gram of gas) of large grains (BGs; dotted line), very small grains (VSGs; dashed line) and PAHs of 100 C atoms (solid line). See text for details.

H Ae stars, such as the shift of the peak positions, but we will limit our discussion to the band strengths.

4. Results

In this section, we describe the results of the calculations and explore the effect of various stellar, disk and PAHs properties.

4.1. Template model

Firstly, we discuss the results for a model that we will use in the following as a template.

The disk is heated by a typical H Ae star with effective temperature $T_{\text{eff}} = 10\,500 \text{ K}$, luminosity $L_{\star} = 32.0 L_{\odot}$ and mass $M_{\star} = 2.4 M_{\odot}$. At a distance of 150 AU the FUV radiation field integrated between 912 and 2050 Å is $\chi = 10^5$ times the average interstellar radiation field ($1.6 \times 10^{-6} \text{ W m}^{-2}$; Habing 1968).

The disk mass is $\sim 0.1 M_{\odot}$. Its inner radius is $R_{\text{in}} = 0.3 \text{ AU}$, close to the BG evaporation radius, the outer radius is $R_{\text{d}} = 300 \text{ AU}$. The surface density profile is $\Sigma = \Sigma_0 \times (r/R_i)^{-1}$ with $\Sigma_0 = 2 \times 10^3 \text{ g cm}^{-2}$. We assume that only half of the star is visible from any point on the disk surface ($\phi_{\star} = 0.5$). Figure 2 shows the run with radius of the pressure (H_p) and photospheric (H_s) scale height and of the flaring angle α (bottom panel). In the top panel we show the temperature of silicates and graphite grains of size $a = 0.01 \mu\text{m}$ at H_s . The gas density at H_s decreases from $7 \times 10^9 \text{ cm}^{-3}$ at R_{in} to $3 \times 10^6 \text{ cm}^{-3}$ at R_{d} .

Each side of the disk intercepts and reprocesses about 10% of the stellar luminosity. The fractional contribution to the reprocessed radiation of BGs, VSGs and PAHs is, respectively, 60%, 13% and 27%. Note that the fraction emitted by PAHs is lower than the fraction of the stellar radiation they absorb

³ To estimate γ , we take $\gamma_0 \sim 3 \times 10^{-6}$ and $f(N_C) \sim 11$ as in Bakes & Tielens (1994).

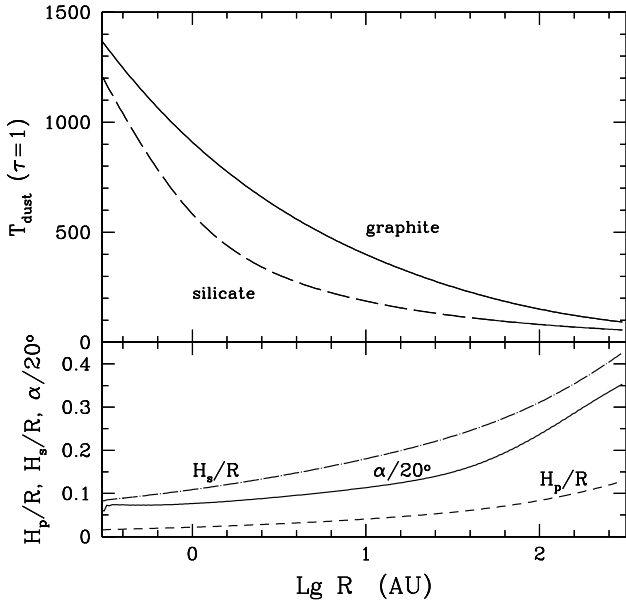


Fig. 2. Disk properties for the template model. The lower panel shows the run with radius of the pressure scale height H_p , the photospheric scale height H_s and the flare angle α divided by 20 deg for convenience. α is 1.4 deg at the inner radius, and reaches 7 deg at the outer disk radius. The top panel shows the temperature for graphite (solid line) and silicate (dashed line) grains of size $0.01 \mu\text{m}$ at H_s .

(about 39%, see preceding section) because of their evaporation in the inner part of the disk. About 10% of the total absorbed flux is lost in PAH evaporation.

Figure 3 shows the calculated spectrum in the 2–40 μm range of a star/disk system seen face-on at a distance of 150 pc. PAH features, which form in the optically thin disk surface, are clearly visible, and some of them are very strong; in Table 3, we give the integrated flux in the 3.3, 6.2, 7.7, 8.6, 11.3, 12.7 and 16.2 μm features after continuum subtraction.

The continuum is mostly due to the large grains which are very hot in the inner regions (see Fig. 2). It is possible to see, for example, the broad feature due to silicate emission peaking at about 10 μm under the much narrower PAH features. Some contribution to the continuum in the wavelength range $\lambda < 10 \mu\text{m}$ is also due to the VSG, as shown by the SED of a model which has all the parameters of the template model but no VSGs nor PAHs (dashed line in Fig. 3).

The PAH emission is much more extended than the adjacent continuum, as shown by two figures, Figs. 4 and 5. Figure 4 plots as function of the projected radius the cumulative intensity of the feature and continuum at 3.3, 6.2 and 11.3 μm . The continuum reaches 50% of its intensity at a very small radius (typically 2–5 AU) while the feature does so at larger radii (about 30 AU for the 3.3 μm feature and 80 AU for the 6.2 and 11.3 μm features). This behaviour basically reflects the different excitation mechanism of PAHs, i.e., single-photon excitation, and of the continuum at the same wavelength, which is dominated by the emission of BGs, in thermal equilibrium with the radiation field. Only very hot BGs, located in the innermost disk, emit at 3 μm whereas PAHs also emit at the outer edge of the disk in the 3.3 μm feature.

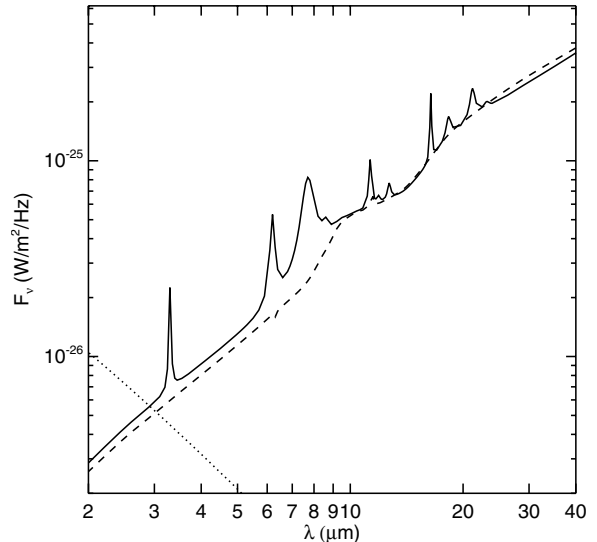


Fig. 3. Spectral energy distribution of a star/disk system (template model) seen face-on at a distance of 150 pc. The solid line shows the emission of the disk, the dotted line that of the stellar photosphere. The dashed line shows the SED of a model which has all the parameters of the template model but no VSGs and no PAHs. The stellar parameters are $T_{\text{eff}} = 10\,500 \text{ K}$, $L_{\star} = 32 L_{\odot}$, $M_{\star} = 2.4 M_{\odot}$. The disk is flared, it has a mass of $0.1 M_{\odot}$, an inner radius of 0.3 AU and an outer radius of 300 AU (see Fig. 2).

The ratio of short wavelength over long wavelength band strength decreases with the intensity of the FUV radiation also for transiently heated particles. Figure 4 shows that the contribution of the outer disk to the 3.3 μm feature is small, while it is much larger for the features at 6.2 and 11.3 μm . We plot for comparison the run with radius of the cumulative fraction of the FUV radiation intercepted by the disk surface. The similar behaviour with the cumulative intensity of the less energetic PAH features reflects the fact that the emission of PAHs roughly scales with the intensity of the FUV radiation field (see Sect. 4.3.1 for more details).

Figure 5 shows the intensity profile obtained by convolving the computed intensity with a two-dimensional gaussian of $FWHM = 0.1''$. As expected from Fig. 4, the features at short wavelengths are strong in the inner hot part of the disk, decreasing rapidly in the outer cold part, whereas those at long wavelengths are weaker in the inner region (mostly because the continuum is higher) but more extended (the temperature required to excite them is lower). In other words, the 3.3 μm probes the inner ($R < 100 \text{ AU}$) region of the disk while the other features probe its outer parts.

4.2. PAH properties

In this section, we investigate the effect of the charge, hydrogenation parameter, size, photoevaporation and absorption cross section of PAHs on the predicted intensity of the features.

4.2.1. Charge state

In Fig. 6, we show the spectra and the brightness distribution for the same model shown in Figs. 3 and 5 but for PAH cations.

Table 3. Predicted strength of the PAH emission features integrated over the disk.

Model	3.3	6.2	7.7	8.6	11.3	12.7	16.4
	[μm]	[μm]	[μm]	[μm]	[μm]	[μm]	[μm]
Template	2.8	5.4	10.2	1.3	2.5	0.6	2.6
Ionized	0.1	7.5	18.2	2.25	0.9	0.13	0.8
$f_{\text{H}} = 0.5$	1.4	5.9	11	1	1.5	0.3	2.6
$N_{\text{C}} = 40$	5.3	2.5	4.1	1.1	10.8	2.8	1
$N_{\text{C}} = 40 - \text{ionized}$	0.3	6.1	12	3	3.9	0.9	0.4

Integrated fluxes (after continuum subtraction) are in units of 10^{-14} W/m^2 .

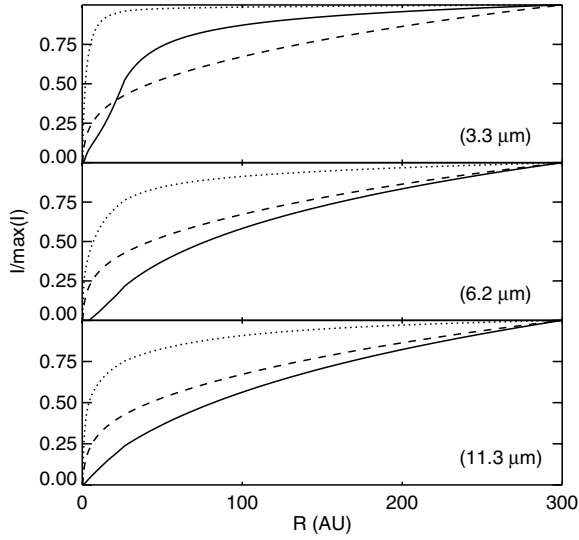


Fig. 4. Cumulative intensity of the feature (continuum subtracted, solid lines) and continuum (dotted lines) at 3.3, 6.2 and 11.3 μm as function of the projected radius. We plot for comparison the run with radius of the cumulative fraction of the FUV radiation intercepted by the disk surface (dashed lines).

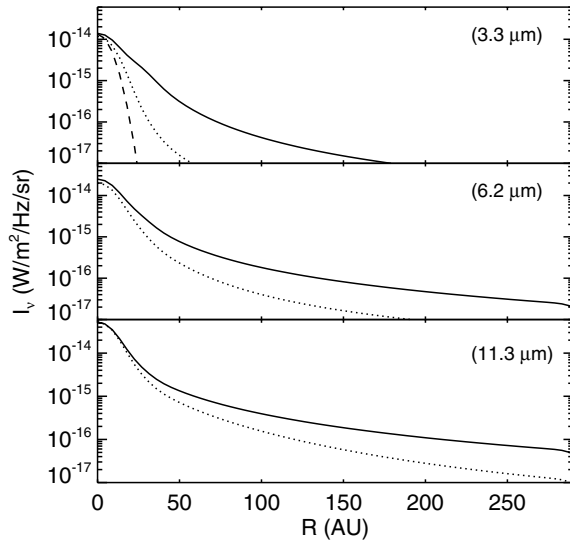


Fig. 5. Surface brightness profiles convolved with a two-dimensional gaussian of $FWHM = 0.1''$ at the peak of the feature (no continuum subtracted, solid lines) and in the adjacent continuum (dotted lines) for the 3.3, 6.2 and 11.3 μm features. In the top panel, we also show the photospheric stellar emission at 3.3 μm convolved with the same beam (dashed line). As in Fig. 3, the star/disk is seen face-on at a distance of 150 pc.

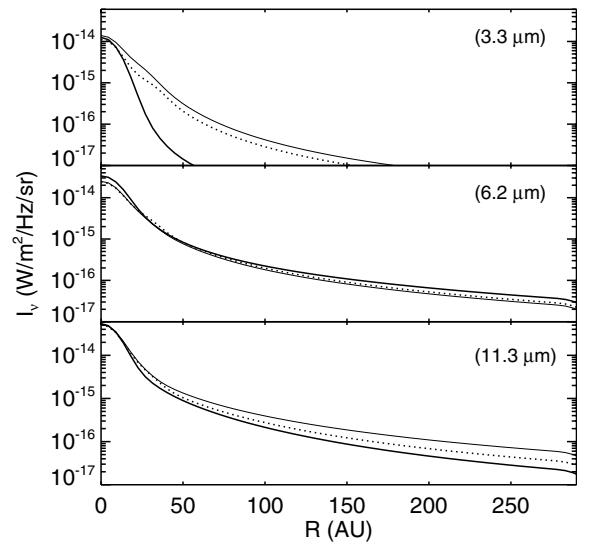
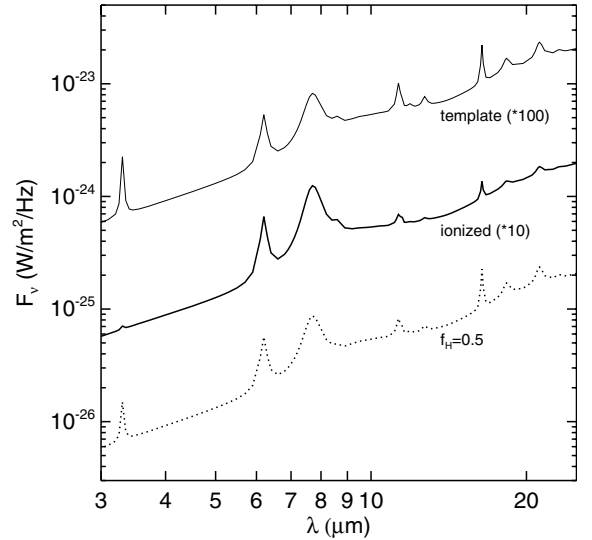


Fig. 6. The top panel shows the SEDs of models containing positively ionized PAH (solid thick line) and partially dehydrogenated PAHs with $f_{\text{H}} = 0.5$ (dotted line). All the other parameters are as in the template model. For comparison, we show again also the SED of the template model (solid thin line). Note that the fluxes of the ionized PAH model and of the template model have been multiplied by factors 10 and 100, respectively. The bottom panel plots the brightness profiles convolved as in Fig. 5 at the peak of the 3.3, 6.2 and 11.3 μm features (no continuum subtracted), as labelled. The lines refer to the ionized PAH model (solid thick), the dehydrogenated PAH model (dotted) and to the template model (solid thin).

The PAH spectrum is a strong function of the PAH charge: the strength of the C-C stretching modes between 6.2 and 8.6 μm is much stronger for ionized PAHs; the 7.7 μm C-C feature to the 11.3 μm C-H feature ratio is increased by a factor of ~ 5 (see Table 3). Further, whereas neutral PAHs show a strong 3.3 μm C-H features, the band almost vanishes when the PAHs are positively ionized.

The IR properties of PAH anions closely resemble those of PAH cations except for the very strong 3.3 μm enhancement in the anion (Szczepanski et al. 1995; Hudgins et al. 2000). However, Bauschlicher & Bakes (2000) predict that PAH anions have band strengths intermediate between those of neutrals (strong 3.3 μm C-H stretching and 11.3, 11.9 and 12.7 μm out-of-plane C-H bending modes) and PAH cations (strong 6.2 and 7.7 μm C-C stretching and 8.6 μm C-H in-plane bending mode).

4.2.2. Hydrogenation parameter

Another effect which can significantly affect the PAH spectra is dehydrogenation. Strong dehydrogenation would make the C-H features disappear. However, theoretical studies of dehydrogenation in the ISM indicate that it is relevant only for the smallest PAHs with $N_C \leq 25$ (Tielens et al. 1987; Allain et al. 1996). Upon absorption of an energetic photon, large PAHs will not have C-H bond rupture since the absorbed energy will promptly be redistributed among many vibrational modes. Nevertheless, in the inner disk regions and for stars with high UV fields dehydrogenation could become important even for large PAHs. To estimate this effect, we run a model with PAHs partially dehydrogenated, i.e., hydrogenation fraction $f_H = 0.5$. The results are shown in Fig. 6. The C-H features (3.3, 8.6, 11.3, 12.7 μm) become lower (by a factor ~ 2 , see Table 3), and the C-C features (6.2, 7.7 μm) become slightly higher (as expected from energy conservation).

4.2.3. Size

We now look at the influence of the PAH size. In Fig. 7 we show a model for smaller PAHs with $N_C = 40$. The relative strength of the PAH emission bands depends strongly on the PAH size: small PAHs radiate strongly at 3.3 μm , while larger (colder) PAHs emit most of their power at longer wavelengths. The 3.3/6.2 μm ratio is ~ 4 times higher for small PAHs than for large PAHs (see Table 3). In addition, since the H/C ratio decreases with the size (see Sect. 3.3), the C-H features increase for small PAHs.

We note that decreasing the PAH size generally goes in the opposite direction than increasing the fraction of ionized PAHs: the emission in the 6–9 μm range decreases for smaller PAHs while for ionized PAHs it increases (see Sect. 4.2.1). On the other hand, the emission at 3.3 and 11.3 μm goes up when PAHs become smaller, whereas it goes down when the fraction of ionized PAHs increases.

Therefore, we expect to find for small *and* ionized PAHs results similar to those predicted by the template model with large and neutral PAHs. For illustration, we show in Fig. 7 a

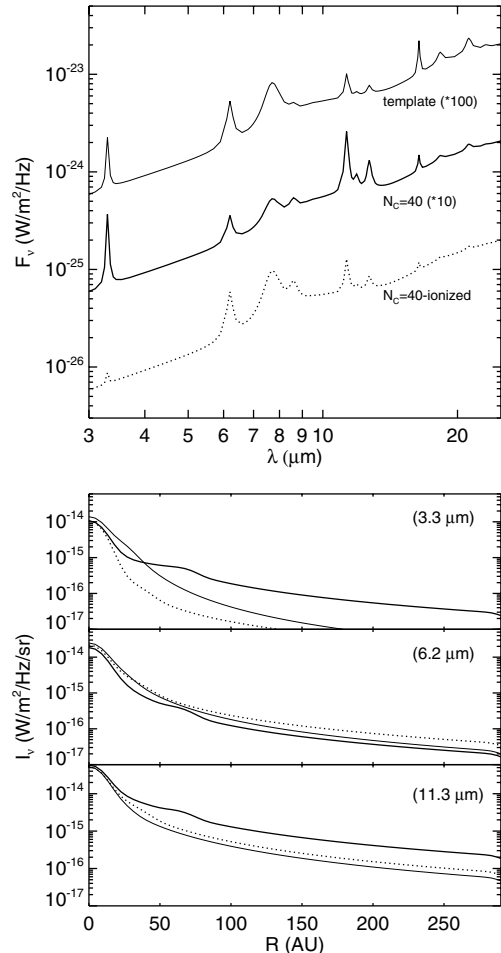


Fig. 7. Same as Fig. 6 for model containing neutral PAHs with $N_C = 40$ (solid thick lines) and ionized PAHs with $N_C = 40$ (dotted lines). Again, we show also the template model by solid thin lines.

model with small ($N_C = 40$) *and* ionized PAHs. In this case, we find in fact that the strength of the 6.2, 7.7 and 11.3 μm features are roughly similar to those predicted by the template model (see Table 3). However, size and ionization do not compensate each other fully and the 3.3 μm band strength is considerably lower (by a factor of 10) than in the template model. But note that for small PAH anions, as mentioned in Sect. 4.2.1, the 3.3 μm feature strength will be higher.

Finally, we find that for small PAHs which are mostly destroyed in the inner (hot) part of the disk – $R \lesssim 70$ AU for $N_C = 40$ – the brightness profiles of the features are affected. The emission is decreased in the inner part and a plateau appears reflecting the compensation between the gradual coming out of PAHs and the decrease of the FUV flux. In the next section, we discuss the photoevaporation effect.

4.2.4. Evaporation

With the formalism adopted here, we find that large PAHs with $N_C = 100$ will not be photo-evaporated in most of the disk, except in the $R > 20$ AU region, while smaller PAHs with $N_C = 40$ will be mostly photo-evaporated in the $R \lesssim 70$ AU region (as mentioned above). Larger PAHs are more stable since

they can easily accommodate the absorbed photon energy. But PAH evaporation, as discussed in Sect. 3.3, is a complex process, and it is possible that our treatment of it underestimates its effects. For stronger photoevaporation, the strength of the most energetic features which come mostly from the inner region will decrease and their brightness distribution will be affected; the effect on the bands at longer λ coming from the outer region will on the contrary be negligible.

On the other hand, it is possible that continuous replenishment of PAHs via sublimation of icy mantles (in which interstellar PAHs may have condensed during the dense molecular cloud phase) or by accreting carbon atoms and/or ions from the gas (see, e.g., Allain et al. 1996) could maintain PAHs throughout the disk. For the template model without evaporation, the strength of the 3.3 μm feature will increase by a factor of ~ 2 while the other features at longer wavelength will not.

4.2.5. Absorption cross section

Finally, we discuss the influence of the absorption cross section. First, the PAH spectra depend on the integrated cross sections of individual features, $\sigma_{\text{IR}}^{\text{int}}$, which, unfortunately, differ among various lab measurements or between experimental and theoretical studies. To get an idea of how these uncertainties affect the PAH spectra we have computed models with enhancement factors of 2–3 in $\sigma_{\text{IR}}^{\text{int}}$. In particular, we have taken for the 6.2, 7.7 and 8.6 μm bands $E_{6.2} = 3$, $E_{7.7} = 2$ and $E_{8.6} = 2$ as suggested by Li & Draine (2001a) in order to fit the 6.2/7.7, 7.7/11.3 and 8.6/7.7 μm band strength ratios observed in ISM spectra. Compared to the template model, the 6.2/7.7 and 7.7/11.3 μm ratios are higher by a factor ~ 2 .

Second, the intensities of the PAH bands depend on the absorption cross section in the visible and UV which are rather uncertain. The cross section ($\sigma_{\text{UV}}^{\text{2D}}$) defined in Sect. 3.3 has been derived for planar PAHs from laboratory measurements of small species ($N_C \leq 30$, Joblin et al. 1992) and, for bigger species, from optical constants for graphite (Verstraete & Léger 1992). However, for astronomical PAHs with more complex 3-dimensional structure very little is known. To estimate the effect of this uncertainty we have computed a model with $\sigma_{\text{UV}}^{\text{3D}}$ for small graphite spheres as in Draine & Lee (1984). The power absorbed by $\sigma_{\text{UV}}^{\text{3D}}$ is ~ 2 times lower than for $\sigma_{\text{UV}}^{\text{2D}}$ and, consequently, the intensity of the features is reduced by ~ 2 .

4.3. Star and disk parameters

The SED of the template model depends not only on the dust model, and in particular on the PAH properties, but also on the star and disk properties. In this section, we investigate the influence of star/disk system parameters on the PAH emission features.

4.3.1. Stellar radiation field

The range of values of the FUV radiation field is large even within the rather limited range of spectral types we investigate in this paper, with χ (the FUV field at a distance of 150 AU

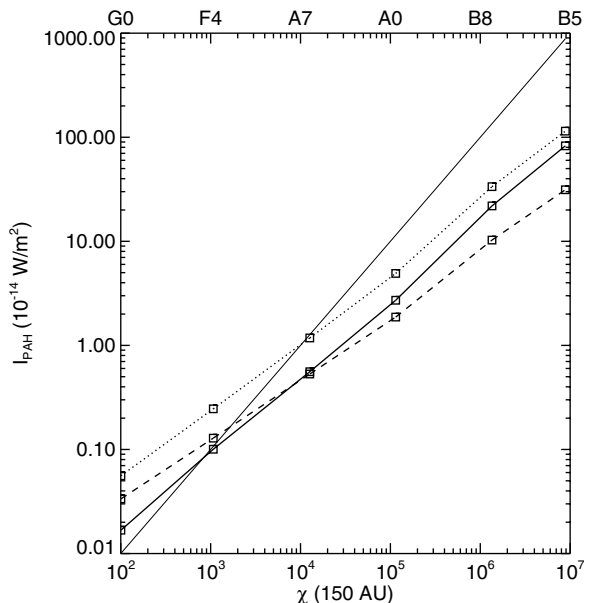


Fig. 8. Strength of the PAH features at 3.3 (solid line), 6.2 (dotted line) and 11.3 μm (dashed line) for ZAMS stars. The scale on the upper axis shows the spectral type, that on the lower axis the corresponding value of χ . The thin solid line shows a linear dependence $I_{\text{PAH}} \propto \chi$. Disk and dust parameters are as in the template model, which has $\chi = 10^5$ ($L_\star = 32 L_\odot$ and $T_{\text{eff}} = 10\,500$ K).

from the star) varying from 10^6 to a few times 10^2 (see Table 1). χ changes because both the luminosity and the effective temperature of the stars change. We have therefore computed a set of disk models for stars of different spectral types assuming that they are on the main sequence, and plotted the results in Fig. 8 as function of the corresponding value of χ . The spectral types are also displayed in the figure.

As expected, the strength of the PAH features increases with χ . The dependence is not linear (see Fig. 8), because the fraction of the stellar radiation absorbed by PAHs depends on its wavelength dependence, i.e., on T_{eff} . For example, the power absorbed by PAHs, normalised by χ , is two times higher for $T_{\text{eff}} = 10\,000$ K than for $T_{\text{eff}} = 15\,000$ and ten times lower than for $T_{\text{eff}} = 6\,000$ K.

Figure 8 shows the intensity of the 3.3, 6.2 and 11.3 μm features as function of χ . One sees that the 3.3 μm one increases faster than the others, since it is the most sensitive to the PAH excitation temperature. One can also note that the competing effect, i.e., the fact that PAH evaporation is larger for higher χ , reducing the 3.3 μm feature more than the others, does not compensate entirely the effect of higher excitation temperatures. However, one should keep in mind that for smaller PAHs ($N_C < 100$), the effect of evaporation could become much larger.

4.3.2. Disk geometry

The dependence of the PAH emission on disk parameters is easily understood. The quantity that most affects the resulting spectrum is the disk flaring angle, which determines at each radius the fraction of FUV intercepted by the disk surface. Lower values of the flaring can be caused by a variety of reasons, for

example if the dust settles toward the disk midplane. Also, if the disk mass is fixed, a steeper dependence of the surface density profile than $p = 1$ tends to make the outer disk less flared, as the ratio of the photospheric to the pressure scale height increases. In all cases, the value of the flaring angle in the inner disk is practically fixed, since it is dominated by its geometrical part (Chiang & Goldreich 1997; Dullemond et al. 2001). Therefore, less flared disks have lower emission in all features, but a higher ratio of the $3.3 \mu\text{m}$ intensity, which forms mostly near the star, where the flaring is dominated by the geometrical part, to that of the 6.2 and $11.3 \mu\text{m}$ ones, which have a much larger contribution from the outer disk. In the extreme case of a geometrically flat disk, the PAH feature strengths decrease by 3 orders of magnitude but the ratio $3.3/11.3 \mu\text{m}$ increases by a factor of 3 and only the $3.3 \mu\text{m}$ band does not completely disappear. The $3.3 \mu\text{m}$ band to continuum ratio decreases by a factor of 4 and becomes equal to 1.1.

In a similar way, when the disk is larger, all features get stronger, but the $3.3 \mu\text{m}$ band less than the others. If R_d becomes very large, the disk turns optically thin to the FUV radiation and the PAH emission does not increase further.

Another parameter to be considered is the disk inclination with respect to the observer. If the disk is inclined it will emit a lower continuum emission at long wavelengths; for an inclination of $\theta = 60 \text{ deg}$ ($\theta = 0$ for face-on disks) the models predict a continuum at $\lambda > 10 \mu\text{m}$ about 20% lower than for face-on models, while at shorter wavelengths there are practically no changes. The continuum-subtracted intensity of all the PAH features we compute will not be affected at all.

A major source of uncertainty in our results derives from the lack of knowledge of the detailed structure of the inner disk. We have assumed in our calculations that the disk is truncated at the dust sublimation radius, and that each disk face is illuminated by 1/2 of the stellar surface. In fact, there is good evidence that in most H Ae stars the disk has a puffed-up rim at the dust sublimation radius, due to the direct illumination of the stellar radiation (Natta et al. 2001; Dullemond et al. 2001). The structure of this rim, and the effects of the shade it projects further out on the disk are rather complex, depending on the detailed 2D radiation transfer for a mixture of grains of different properties. The correct treatment of the effects of this region on the PAH emission is well beyond the current capabilities of our models. However, we can make some qualitative estimates in the following way. A puffed-up inner rim will emit a strong continuum at short wavelengths. This affects mainly the ratio of the $3.3 \mu\text{m}$ band to the continuum; considering that models that include the rim predict a $3.3 \mu\text{m}$ continuum a factor of ~ 3 larger than our models (see Natta et al. 2001), the $3.3 \mu\text{m}$ peak to continuum ratio will decrease by a factor of 2. However, the continuum-subtracted intensity of the $3.3 \mu\text{m}$ feature will not be affected; also, the effect on the other features at longer wavelength is negligible.

The geometrical effect of the rim on the disk illumination can be much smaller than we have assumed by taking $\phi_\star = 0.5$, to the limit of being entirely negligible. In this case, each point on the disk will be illuminated by the entire stellar surface, and the fraction of intercepted stellar radiation will increase by a factor of 2 with respect to our template model.

We have checked that this results, with a large degree of accuracy, in a factor of 2 increase of all the strong PAH features. The total IR excess will also be a factor of 2 larger, going from about 20%, for a face-on disk, to about 40%. Most H Ae stars have indeed an IR excess within this interval (Meeus et al. 2001; Dullemond & Natta 2003), and one expects that more realistic models will be roughly intermediate between these two cases. However, it should be noted that one can expect also some modest change in the ratio of features at different wavelengths, as the rim shade will affect different regions of the disk differently.

5. Comparison with the observations

A first test of our models can be made by comparing the predicted intensity of the most commonly observed PAH features (i.e., at 3.3 , 6.2 and $11.3 \mu\text{m}$) with the observations. We do that in Fig. 9, which plots for each feature the intensity normalized to the FUV flux of the star, as function of the value of χ (i.e., the FUV field at 150 AU from the star). Both quantities are distance-independent. The solid lines show the prediction of models for main-sequence stars of different spectral type (and χ), as described in Sect. 4.3.1. The lower line refers to models where $\phi_\star = 0.5$, the upper lines to models with $\phi_\star = 1$. The thin lines show an uncertainty strip of \pm a factor of 2 around these models. This, as we have discussed, is a conservative estimate of the uncertainties due to deviations from the assumptions of the template models, in the disk description (different surface density profiles, flaring etc.) and in the assumed dust model.

5.1. PAHs in disks: Consistent with observations?

In the following, in order to see if PAHs in disks are consistent with observations, we check for each star group described in Sect. 2 if the disk models can account for the observed PAH intensities.

5.1.1. Flared disks

Objects with flared disks, according to the classification of Meeus et al. (2001) (group I) are marked as crosses in Fig. 9. This group dominates among the detections, as expected from our models. They are in general well accounted for by disk models with “standard” dust, as defined in Sect. 3.3. This is true also for the two younger sources, i.e., HD 97048 and Elias 1 (shown by triangles), especially if we correct for contamination in the two longer wavelength bands by the associated reflection nebula (about $\sim 40\%$ for HD 97048; van Boekel et al. 2004). We also show by asterisks the H AeBe stars observed by Brooke et al. (1993) at $3.3 \mu\text{m}$. They cover a range of χ from about 10^4 to very high values ($\sim 10^6$), and we do not have detailed information on their disk properties. However, the objects with $\chi \lesssim 10^4$ are consistent with our disk predictions. No upper limit in objects with $\chi \lesssim 10^5$ is significantly lower than the model predictions.

In 8 of these objects one has a measurement (or significant upper limit) of both the 3.3 and the $6.2 \mu\text{m}$ features. The ratio

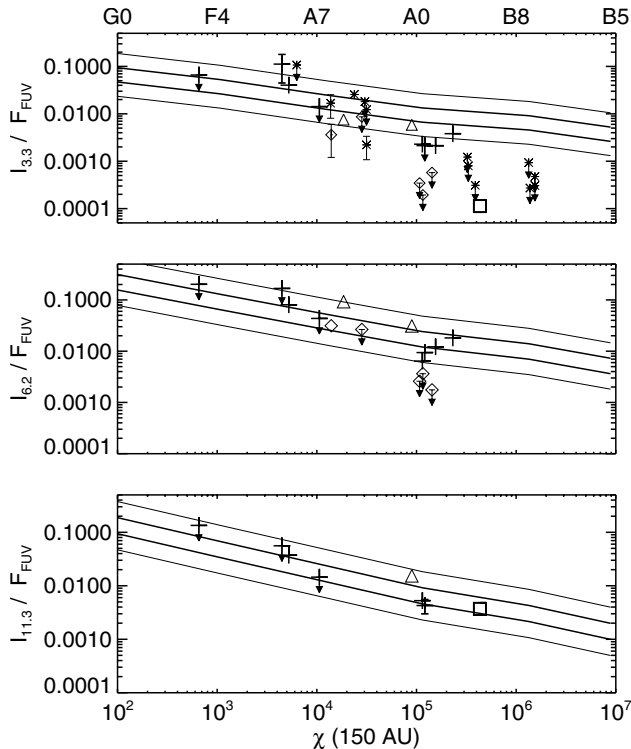


Fig. 9. Comparison of model predictions and observations. *Upper Panel:* Strength of the $3.3 \mu\text{m}$ feature normalised to the FUV flux of the star for ZAMS stars. As in Fig. 8, the scale on the upper axis is the spectral type, that on the lower axis is the value of χ , i.e., the FUV field at 150 AU from the star. The two solid lines show the predictions of the template model for $\phi_{\star} = 0.5$ (lower curve) and $\phi_{\star} = 1.0$ (upper curve) (see text). The two thin lines show an uncertainty strip of \pm a factor of 2 around these models. The crosses show observed intensities (normalized to the corresponding FUV flux) for the isolated HAeBe stars with evidence of a flared disk, the diamonds for the isolated HAeBe stars with no evidence of a flared disk and the triangles for the intermediate sources (HD 97048 and Elias 1). The asterisks show the HAeBe stars observed from the ground by Brooke et al. (1993); the square is WL 16, corrected for dust attenuation (see text). Error bars, when not shown, are smaller than the symbols. Arrows are 5σ upper limits. *Medium and lower Panels:* Same as upper panel for the 6.2 and $11.3 \mu\text{m}$ feature.

ranges from 0.1 to about 0.5, somewhat lower than the value predicted by the model of 0.5 ± 0.2 . In four cases, one can also measure the ratio of the 11.3 to the $6.2 \mu\text{m}$ feature. The values are about 0.5 in 3 cases, and 0.8 (with an uncertainty of ± 0.2) in the fourth object, in good agreement with the template model predictions of 0.4 ± 0.2 . It is likely, as we will discuss further in Sect. 5.3, that our models tend to overestimate the intensity of the $3.3 \mu\text{m}$ feature by a factor 2–3 in stars with $3 \times 10^4 \leq \chi \leq 3 \times 10^5$.

However, there are two groups of non-detections that are interesting. We discuss these in the following.

5.1.2. Flat disks

The first is the group of 5 diamonds, i.e., HAeBe stars with no evidence of a flared disk (group II, Meeus et al. 2001). Of these, only in one case (HD 142666) PAHs have been detected

at 3.3 and $6.2 \mu\text{m}$; most of the non-detections are well below the model predictions. This agrees quite well with our result that flat disks should have very weak PAH features, even when PAHs are present with normal properties on the disk surface.

5.1.3. High- χ stars

Other interesting objects are those with high values of χ ($> 3 \times 10^5$). Most of them (the exception being WL 16, which we discuss in more detail in the following) are from Brooke et al. (1993), and only the $3.3 \mu\text{m}$ feature has been observed. All these objects with high χ have $3.3 \mu\text{m}$ intensities (or upper limits) well below the model predictions.

The interpretation of this group of objects is not straightforward; it is quite possible that their disks, if they ever existed, have been dissipated by the strong radiation field of the star (Natta et al. 2000; Fuente et al. 2002), or that they are flat (Hillenbrand et al. 1992). There are, however, other possibilities. One is that the abundance of PAHs is lower than we assumed. Photoevaporation, which increases rapidly with χ and for smaller PAHs, could easily reduce the PAH abundance well below our assumed value. PAH evaporation, as discussed in Sect. 3.3, is a complex process, and we may have underestimated its effects.

It is also possible that the PAHs are ionized and/or dehydrogenated in the inner disk region, resulting in a much reduced $3.3 \mu\text{m}$ band (see Sects. 4.2.2 and 4.2.1). Observations of the PAH emission from WL 16, shown by a square in Fig. 9⁴, favors this last possibility. In fact, we find that while the models reproduce well the $11.3 \mu\text{m}$ feature strength, that of the $3.3 \mu\text{m}$ feature is well below the predictions. Moreover, Ressler & Barsony (2003) interpret the spatial variation of the 7.7 (or 8.6)/ $11.3 \mu\text{m}$ flux ratio as due to a change of the PAH charge state along the disk. In the inner region PAHs appear to be positively charged while in the outer region they are neutral. Furthermore, the $12.7/11.3 \mu\text{m}$ flux ratio, which increases in the outer part of the disk, could indicate the presence of more hydrogenated PAHs in the outer part.

5.2. Which PAHs?

As we have just seen, our template model with relatively large ($N_C = 100$) neutral PAHs fits very well the strength of the most commonly observed features, with the possible exception of the $3.3 \mu\text{m}$ one, which tends to be much lower than predicted in stars with $\chi \geq 3 \times 10^5$.

In stars with lower χ (spectral type roughly later than B9), we can rule out that PAHs are large and ionized, because they will produce too low $3.3/6.2$ and $11.3/6.2 \mu\text{m}$ ratios (by a factor of >10 and 4 , respectively, see Sect. 4.2.1 and Table 3). Similarly, large and strongly dehydrogenated PAHs are unlikely, since they will also produce too low $3.3/6.2$ and $11.3/6.2 \mu\text{m}$ ratios (see Sect. 4.2.2). Further, we can rule

⁴ In Fig. 9, the data for the embedded young stellar object WL 16 have been corrected for dust attenuation taking a visual extinction of $A_V = 31$ from Ressler & Barsony (2003) and using the extinction coefficient of Draine & Lee (1984); Draine (1989).

out that PAHs are much smaller than our assumed model ($N_C = 100$), because they will produce too high 3.3/6.2 and 11.3/6.2 μm ratios (by a factor of 4 and 10, respectively, see Sect. 4.2.3 and Table 3).

On the other hand, we cannot exclude that PAHs are small *and* ionized. In this case, we find that the strength of the 6.2 and 11.3 μm features, as well as their ratio will be roughly similar to the values predicted by the template model with large and neutral PAHs (see Sect. 4.2.3). This is easily understood considering that the effects of size and ionization compensate each other. For small positively charged PAHs the compensation is nevertheless not complete, and, the intensity of the 3.3 μm feature will be lower than in the template model by a factor ~ 10 (see Table 3). Therefore, this model, which underestimates the 3.3 μm feature strength by a factor of 3 in stars with $3 \times 10^4 \leq \chi \leq 3 \times 10^5$ but by a much larger factor in stars with $\chi \leq 3 \times 10^4$, seems unlikely. For small negatively charged PAHs the 3.3 μm feature is expected to be stronger (see Sect. 4.2.1) and could become comparable to the observations. However, it is difficult to assess the reliability of this model, since the IR properties of PAH anions are not well known.

To get some additional insight into the PAH properties, one can look at the other weaker PAH features (i.e., 8.6, 12.7 or 16.4 μm) even if they have been only sporadically detected. This is probably due to the low S/N ratio of the spectra. The models with large neutral PAHs and small ionized PAHs predict similar strengths of the 8.6 and 12.7 μm features, in good agreement with observations (see Tables 2 and 3). On the other hand, large neutral PAHs will produce a 16.4 μm feature five times stronger than small ionized PAHs. This favors the small ionized PAHs model since this feature has not been detected in the ISO spectra of isolated HAeBe stars (Van Kerckhoven et al. 2002). However, high S/N spectra in this wavelength region are needed to determine the properties of the carrier of this band.

The large and neutral PAH hypothesis is supported by the detailed studies of the PAH spectra in HAeBe stars based on both laboratory data and theoretical calculations (Hony et al. 2001; Van Kerckhoven et al. 2002; Peeters et al. 2002). Together with the comparison of the PAH profiles observed in evolved stars and ISM-like sources, they indicate that PAHs should be larger and less ionized in isolated HAeBe stars, in agreement with our template model.

It must be emphasized that there are several complications that we have neglected in this study. The most obvious is that we have assumed that PAHs can be characterized by a single size and charge state. This is unlikely to be the case, and one can expect variations as a function of radius and depth in the disk, as well as from object to object. For example, PAHs are likely to be more positively ionized in the inner disk region and for stars with higher χ . This could explain the gradual decrease of the 3.3 μm feature strength with χ seen in Fig. 9. In stars with $3 \times 10^4 \leq \chi \leq 3 \times 10^5$ it is possible that we have an *intermediate* situation, and in fact a model with a mixture of both large neutral and small ionized PAHs will predict a 3.3 μm feature strength lower than in the template model by a factor of 2–3, close to the observed values.

We conclude that in stars with $\chi \leq 10^5$ PAHs may be preferentially relatively large ($N_C \geq 100$) and neutral. But small *and*

negatively ionized PAHs can also reproduce the observations. For comparison, Li & Lunine (2003), who have modelled the emission features from the (debris) disk around HD 141596A (with $\chi = 10^5$) conclude that PAHs must be mostly negatively charged. However, they show that models consisting of a mixture of both neutral and charged PAHs are also capable of reproducing the observations. For stars with $\chi > 10^5$, the large neutral PAH model tends to overestimate the intensity of the 3.3 μm feature. This could result from changes in the disk structure (e.g., disks may have dissipated), or from changes in the characteristics of the PAHs, which can be ionized, dehydrogenated or strongly photoevaporated in the inner disk regions.

From the integrated spectra, it is difficult to discriminate between the various effects due to ionization, dehydrogenation or evaporation. To provide better insight into evolution of PAH properties within the disk, high angular spatial spectroscopic observations in the bands are needed.

6. Summary

We have investigated the emission from PAHs on the surface of disks around HAeBe stars by comparing model predictions with observations. We have computed models of disks, heated by irradiation from the central source, that contain large grains, in thermal equilibrium with the radiation field, and transiently heated very small grains and PAHs. The disks are optically thick to the stellar radiation, in hydrostatic equilibrium in the vertical direction, with dust and gas well mixed (flared disks). We have used a 2-layer model to calculate the disk structure and implement a 1D radiative transfer code to compute the emerging spectrum. This scheme is reliable and efficient (see Sects. 3.1 and 3.2). Our main results can be summarized as follows.

1. The models predict an infrared SED showing PAH features at 3.3, 6.2, 7.7, and 11.3 μm clearly visible above the continuum. The PAH emission, spatially extended, comes mostly from the outer disk region ($R \sim 100$ AU) while the continuum emission at the same wavelength, mostly due to warm large grains, is confined to the innermost disk regions ($R \sim \text{few AU}$). Among the PAH features, the 3.3 μm one is the least extended; in our template model, about 1/2 of its integrated intensity comes from $R < 30$ AU.
2. From comparison with ISO and ground-based observations, we find that most of the observed PAH features in objects with flared disks (group I, Meeus et al. 2001) are well described by our models. In objects with no evidence of a flared disk (group II, Meeus et al. 2001) no (or weak) PAH features have been detected, as expected from our models. For geometrically flat disks, PAH features are predicted to be very weak, even when PAHs with standard properties are present on the disk surface.
3. Objects with a strong radiation field (spectral type generally earlier than about B9) have a 3.3 μm feature (often the only one observed) much weaker than predicted. We suggest that their disks have been dissipated by the strong radiation field, or that PAHs have been photoevaporated more effectively than our model predicts, or that their properties

(ionization or dehydrogenation) have been modified in the inner disk region. All these scenarios will cause the $3.3 \mu\text{m}$ feature to practically disappear.

4. Finally, we find that in circumstellar disks around stars with spectral type later than B9, PAHs should have an abundance typical of the ISM. They may be preferentially large and neutral, or small and ionized, and integrated spectra alone cannot distinguish between these two possibilities. To provide better insight into the PAH properties evolution within the disk, high angular resolution spectroscopic observations are needed. The fact that we can explain the observed PAH spectra, at least of the isolated H Ae stars, with PAH abundances and qualitative properties similar to those of PAHs in the ISM is interesting. It seems that, if PAHs are re-formed in disks, after having been depleted (by coagulation or other processes) in dense cores, they again contain roughly the same amount of carbon (relative to that of large grains) that they contain in the ISM. This is a very interesting point, which certainly deserves further attention.

To the best of our knowledge, this study represents the first successful modeling of the PAH emission features from disks around pre-main-sequence stars. It shows that PAHs are present in disks, at least around H AeBe stars, and absorb a significant fraction of the stellar radiation, similarly to PAHs in the ISM. Consequently, PAHs are an important source of opacity in circumstellar disks and are likely to play a dominant role in the thermal budget and chemistry of the gas. The coupling between PAHs and gas can determine the gas temperature in the outer disk regions, where the lower density can make the collisional coupling between gas and grains inefficient, and as a consequence have a significant impact on the disk structure itself. Finally, as a side aspect, PAH emission, which is sensitive to the local physical conditions – either directly or through a change of their physical characteristics – could be useful for a better understanding of the physical conditions prevailing in the surface of circumstellar disks. Furthermore, PAH emission, which is more extended than the thermal emission at similar wavelengths, can offer a unique possibility to probe the outer disk structure.

Acknowledgements. We are grateful to F. Boulanger and L. Verstraete for fruitful discussions and relevant comments and suggestions.

References

- Allain, S., Bouvier, J., Prosser, C., Marschall, L. A., & Laaksonen, B. D. 1996, *A&A*, 305, 498
- Bakes, E. L. O., & Tielens, A. G. G. M. 1994, *ApJ*, 427, 822
- Bauschlicher, C., & Bakes, E. 2000, *J. Chem. Phys.*, 262, 285
- Berrilli, F., Corciulo, G., Ingrassio, G., et al. 1992, *ApJ*, 398, 254
- Boulanger, F., & Perault, M. 1988, *ApJ*, 330, 964
- Brooke, T. Y., Tokunaga, A. T., & Strom, S. E. 1993, *AJ*, 106, 656
- Chiang, E. I., & Goldreich, P. 1997, *ApJ*, 490, 368
- Désert, F. X., Boulanger, F., & Puget, J. L. 1990 *A&A*, 237, 215
- Dominik, C., Dullemond, C. P., Waters, L. B. F. M., & Walch, S. 2003, *A&A*, 398, 607
- Draine, B. T., & Lee, H. M. 1984, *ApJ*, 285, 89
- Draine, B. T. 1985, *ApJS*, 57, 587
- Draine, B. T. 1989, In *Infrared Spectroscopy in Astronomy*, 93
- Dullemond, C. P., & Natta, A. 2003, *A&A*, 408, 161
- Dullemond, C. P., Dominik, C., & Natta, A. 2001 *ApJ*, 560, 957
- Dwek, E., Arendt, R. G., Fixsen, D. J., et al. 1997, *ApJ*, 475, 565
- Fuente, A., Martin-Pintado, J., Bachiller, R., Rodriguez-Franco, A., & Palla, F. 2002 *A&A*, 387, 977
- Geballe, T. R. 1997, In *From Stardust to Planetesimals*, 119
- Grady, C. A., Polomski, E. F., Henning, T., Stecklum, B., & Woodgate, B. E. 2001, *AJ*, 122, 3396
- Guhathakurta, P., & Draine, B. T. 1989, *ApJ*, 345, 230
- Habart, E., Verstraete, L., Boulanger, F., et al. 2001, *A&A*, 373, 702
- Habart, E., Boulanger, F., Verstraete, L., Walmsley, C. M., & Pineau Des Forêts, G. 2004, *A&A*, 414, 531
- Habing, H. J. 1968, *Bull. Astron. Inst. Netherlands*, 19, 421
- Hanner, M. S., Tokunaga, A. T., & Geballe, T. R. 1992, *ApJ*, 395, L111
- Hanner, M. S., Brooke, T. Y., & Tokunaga, A. T. 1994 *ApJ*, 433, L97
- Hillenbrand, L. A., Strom, S. E., Vrba, F. J., & Keene, J. 1992, *ApJ*, 397, 613
- Hony, S., Van Kerckhoven, C., Peeters, E., et al. 2001, *A&A*, 370, 1030
- Hudgins, D. M., Bauschlicher, C., Allamandola, L. J., & Fetzer, J. 2000, *J. Chem. Phys.*, 104, 3655
- Joblin, C., Léger, A., & Martin, P. 1992, *ApJ*, 393, L79
- Li, A., & Draine, B. T. 2001a, *ApJ*, 554, L778
- Li, A., & Draine, B. T. 2001b, *ApJ*, 550, L213
- Li, A., & Lunine, J. I. 2003, *ApJ*, 594, 987
- Malfait, K., Waelkens, C., Waters, L. B. F. M., et al. 1998, *A&A*, 332, L25
- Meeus, G., Waters, L. B. F. M., Bouwman, J., et al. 2001, *A&A*, 365, 476
- Moore, T. J. T., Emerson, J. P., Skinner, C. J., et al. 1998, *MNRAS*, 299, 1209
- Natta, A., & Testi, L. 2003, In *Star Formation in the Interstellar Medium*, PASP
- Natta, A., Grinin, V., & Mannings, V. 2000, in *Protostars and Planets IV*, 559
- Natta, A., Prusti, T., Neri, R., Wooden, D., Grinin, V. P., & Mannings, V. 2001, *A&A*, 371, 186
- Omont, A. 1986, *A&A*, 164, 159
- Peeters, E., Hony, S., Van Kerckhoven, C., et al. 2002, *A&A*, 390, 1089
- Ressler, M. E., & Barsony, M. 2003, *ApJ*, 584, 832
- Schutte, W. A., Tielens, A. G. G. M., Allamandola, L. J., Wooden, D. H., & Cohen, M. 1990, *ApJ*, 360, 577
- Siebenmorgen, R., Kruegel, E., & Mathis, J. S. 1992, *A&A*, 266, 501
- Siebenmorgen, R., Prusti, T., Natta, A., & Muller, T. G. 2000, *A&A*, 361, 258
- Siebenmorgen, R. 1993, *ApJ*, 408, 218
- Snow, T. P., & Witt, A. N. 1995, *Science*, 270, 1455
- Szczepanski, J., Wehlburg, C., & Vala, M. 1995, *Chem. Phys. Lett.*, 232, 221
- Testi, L., Palla, F., & Natta, A. 1998, *A&As*, 133, 81
- Tielens, A. G. G. M., Allamandola, L. J., Barker, J. R., & Cohen, M. 1987, In *Polycyclic aromatic hydrocarbons and astrophysics*, 273
- Tokunaga, A. T., Sellgren, K., Smith, R. G., et al. 1991, *ApJ*, 380, 452
- van Boekel, R., Waters, L. B. F. M., Dominik, C., et al. 2004, *A&A*, 418, 177
- Van Kerckhoven, C., Tielens, A. G. G. M., & Waelkens, C. 2002, *A&A*, 384, 568
- Verstraete, L., & Léger, A. 1992, *A&A*, 266, 513
- Weingartner, J. C., & Draine, B. T. 2001, *ApJS*, 134, 263

Online Material

Appendix: Numerical method for radiation transfer

The disk is divided into rings of radius r and small radial width Δr . At the center, at $r = 0$, sits the star with parameters M_\star , L_\star , R_\star and T_{eff} . For each ring we compute, as described below, the radiative transfer perpendicular to the disk, in the z -direction, and then add up the contributions from all rings.

Each ring is treated as a plane-parallel slab. It displays mirror symmetry with respect to the mid-plane at $z = 0$. We solve the integral equations

$$I^+(\tau) = e^{-\tau} \left(I^+(0) + \int_0^\tau S(x) e^x dx \right) \quad (1)$$

$$I^-(\tau) = e^{-\tau} \left(I_0 + \int_0^\tau S(x) e^x dx \right). \quad (2)$$

$I^+(\tau)$ is the intensity at optical depth τ and frequency ν in the upward direction along a straight line under an angle $\mu = \cos \theta$ with respect to the z -axis; τ is zero at $z = 0$. The second equation containing I^- refers to downward beams. I_0 is the radiation intensity that falls on the disk from outside (the star). The indices θ and ν have been dropped for convenience of writing. $S(\tau)$ is the source function. The optical thickness τ and geometrical height z are related through $d\tau = \rho \kappa dz$ where ρ is the mass density and κ the mass extinction coefficient of dust.

There are two boundary conditions. One states that at the top of the slab the incoming intensity $I^- = I_0$ is zero except towards the star where it equals $B_\nu(T_{\text{eff}})$. The stellar hemisphere, which seen from a distance r subtends a solid angle $\Omega = \pi R_\star^2 / 2r^2$, is replaced by a luminous band of the same intensity $B_\nu(T_{\text{eff}})$. The band encircles the sky at an elevation α and has a width $\Omega / 2\pi \ll \alpha$, its solid angle is also Ω . The other boundary condition reads $I^+ = I^-$ at $z = 0$.

One starts the calculation of the radiative transfer for a ring with a guess for the vertical dust temperature profile $T(z)$. This fixes the source function $S(\tau)$ once the dust properties have been specified. Then one solves (1) and (2) for $I_\nu^+(z, \mu)$ and $I_\nu^-(z, \mu)$ and calculates from I^+ , I^- the mean intensity of the radiation field $J(z)$. This makes it possible to compute a new temperature run $T(z)$. The procedure is iterated until $T(z)$ converges.

Because in our examples the visual opacity of the disk in z -direction can be very large ($> 10^5$), we apply the following slight modification to what we said above. We slice the disk into a completely opaque mid-layer sandwiched between two thin top layers. The mid-layer, because of its high optical

depth and the lack of internal energy sources, is considered to be isothermal at temperature T_{mid} ; the value depends, of course, on r . We evaluate the radiative transfer for the top layer according to the method described before, and separately for the isothermal midlayer, but there it is trivial. A boundary condition connects the two layers. In the calculation for the top layer, we now position the zero point of the z -axis at the transition between top and mid-layer. The intensity that enters the top layer from below in the direction $\mu = \cos \theta$ is

$$I_\nu^+(z = 0, \mu) = B_\nu(T_{\text{mid}}) \left(1 - e^{-\tau_\nu(\mu)} \right). \quad (3)$$

Here $\tau_\nu(\mu)$ is the optical depth of the mid-layer. The monochromatic flux received by the top layer from below is therefore

$$F_\nu = 2\pi B_\nu(T_{\text{mid}}) \int_0^1 \left(1 - e^{-\tau_\nu(\mu)} \right) \mu d\mu. \quad (4)$$

The frequency integral $\int f_\nu d\nu$ must be equal to the downward flux at $z = 0$ because the net flux, for reasons of disk symmetry, vanishes everywhere. This condition yields T_{mid} , of course, iteratively. In mathematical form, it reads

$$\int d\nu B_\nu(T_{\text{mid}}) \int_0^1 d\mu \left(1 - e^{-\tau_\nu(\mu)} \right) \mu = \int d\nu \int_0^1 d\mu \mu I_\nu^-(z = 0). \quad (5)$$

Ideally, the top layer extends downwards so deep that the temperature at its bottom asymptotically approaches the temperature of the mid-layer, T_{mid} . Then the whole disk of arbitrary thickness is calculated consistently. But that would require a visual optical depth of the top layer in the z -direction, τ_{top} , of several hundred and therefore many (hundreds of) vertical grid points. In practice, we have found that $\tau_{\text{top}} \simeq 4$ is sufficient, since practically all starlight is absorbed and $T(z = 0)$ is very closed to T_{mid} . Typically, changing τ_{top} from 4 to 40 changes the emerging SED by less than 20% at all wavelengths.

We wish to make a few further points: *a*) the radiation that is absorbed in the top layer and then reemitted at infrared wavelengths may leave the top layer, be again scattered or absorbed there, or may enter the mid-layer. *b*) The net flux is always zero, but the upward and downward integrated fluxes, F^+ and F^- , do depend on z , so always $F^+ + F^- = 0$, but $dF^+/dz \neq 0$. *c*) Good agreement in the results of our radiative transfer code with another one is demonstrated on the URL address <http://www.mpa-garching.mpg.de/dullemon/radtrans/benchmarks>